Journal of Luminescence 202 (2018) 168–175

Contents lists available at ScienceDirect

Journal of Luminescence

journal homepage: www.elsevier.com/locate/jlumin

Blue-yellow emission adjustability with aluminium incorporation for cool to warm white light generation in dysprosium doped borate glasses

Simranpreet Kaur[a], Deepawali Arora[a], Sunil Kumar[b], Gurinderpal Singh[b], Shaweta Mohan[c], Puneet Kaur[d], Kriti[a], Puneet Kaur[a], D.P. Singh[a,*]

[a] Department of Physics, Guru Nanak Dev University, Amritsar 143005, India
[b] Department of Physics, Khalsa College, Amritsar 143005, India
[c] Department of Physics, BBK DAV College Amritsar 143005, India
[d] Department of Mathematics, Guru Nanak Dev University, Amritsar 143005, India

ARTICLE INFO

Keywords:
Energy transfer
Optical properties
Activators, warm White LED glasses

ABSTRACT

A series of white light emitting Dy^{3+} doped lead borate (DY) and lead alumino borate (DYA) glasses have been prepared by melt quench technique and are explored by XRD, FTIR, optical absorptions, fluorescence and density measurements. In this paper an effort has been made to compare the structural changes and luminescence efficiencies of prepared glasses by changing dysprosium oxide content and glass network environment by adding aluminium oxide. The XRD profile of all the glasses confirms their amorphous nature and FTIR study shows the presence of BO_3 and BO_4 groups. Incorporation of Al_2O_3 in the glass system is responsible for a strong effect on luminescence of the present glass system. There is a strong correlation between Dy^{3+} ions concentration and the host glass composition on the energy transfer mechanism. The decay curves deviate gradually from single exponential function at lower concentrations to non-exponential behavior at higher concentrations. The Inokutie Hirayama (IH) model for S= 6 fits well the non-exponential decay curves that indicate dipole-dipole type energy transfer between donor and acceptor ions. The calculated chromaticity coordinates lie in the white region of CIE 1931 chromaticity diagram and are in excellent proximity with the standard equal energy white illuminant (0.333, 0.333). Furthermore, the calculated correlated color temperature and the yellow to blue (Y/B) ratio of the synthesized photonic glasses may offer the possibility of tuning the white light by varying concentration and host environment which could be useful for various photonic based device applications.

1. Introduction

Rare earth ions are widely studied in various crystalline and glassy systems. They play an eminent role in the development of number of optoelectronic devices such as lasers, sensors, light converters, hole burning high density memories, optical fibres and amplifiers [1–3]. Glasses incorporated with rare earth ions have been developed as promising host materials for lasing phenomenon owing to their suppleness of shape, size, transparency and ease of fabrication over their crystalline competitors. Recently, white light emitting diodes (WLEDs) have gained a lot of attention as they are promising candidates in place of conventional incandescent and fluorescent lamps, due to their less energy consumption and environmental benefits. Rare earth doped white color luminescence glass systems have some assorted advantages such as consistent light emission, easy manufacture, cheap fabrication cost and high thermal stability. White light emitting glasses has formally been developed by Zhang et al. [4] in 1991 and have attracted a lot of interest in current years [5–7]. The visible luminescence of the Dy^{3+} ion comprises of two strong bands one in blue and the other in yellow regions corresponding to $^4F_{9/2}\rightarrow{}^6H_{15/2}$ and $^4F_{9/2}\rightarrow{}^6H_{13/2}$ transitions respectively. At an appropriate yellow to blue Y/B intensity ratio, Dy^{3+} ions are known to radiate white light. So, the luminescent materials doped with Dy^{3+} ions are used as two-band or white light phosphors [8,9]. Liu et al. [5] reported that the $CaO\text{-}B_2O_3\text{-}SiO_2$ glass doped with Dy^{3+} ions shows chromaticity coordinates in the white light region. Using the melt-quenching technique, Dy^{3+}doped lead phosphate [6] and lithium borate [7] glasses are prepared and characterized for white LED applications. For the similar applications, Leow et al. [8] prepared and studied the optical properties of $BaB_2Si_2O_8$ phosphor glasses doped with Dy^{3+} ions which showed blue and green emissions in the Photoluminescence (PL) spectrum. The white-emitting $Sr_3Y(PO_4)_3$: Dy^{3+} doped phosphors have been synthesized by Seo et al. [9], its emission properties are tuned by varying the concentrations of Dy^{3+} ions from 2% to 18% mol.

* Corresponding author.
E-mail address: dpsinghdr@gmail.com (D.P. Singh).

https://doi.org/10.1016/j.jlumin.2018.05.034
Received 31 January 2017; Received in revised form 9 May 2018; Accepted 10 May 2018

Heavy metal oxide (HMOs). [10,11] based rare earth doped glass systems have high lasing potencies due to their large mass, low field strength and high polarizability. Borate glasses incorporated with heavy metal oxides have been known to give strong fluorescence in the visible spectral region which is used as electro-optic modulators, electro-optic switches, solid state laser materials and non-linear parametric converters [12,13]. Another significant feature of borate glasses is the modifications in its structural properties with the addition of modifiers or intermediates. The network of the borate glasses are formed by gathering of BO_3 triangles and BO_4 tetrahedra units to form well defined and stable borate groups such as diborate, triborate, tetraborate etc., that constitute the random three-dimensional network of these stable groups rather than there random distribution in the network. The B_2O_3 based glasses are well known for their large (even larger than crystals) photo induced second order non-linear optical effects owing to a strong effect on luminescent efficiencies of these glasses [14]. Many researchers reported concentration quenching of photoluminescence at large doping concentration (greater than 1.0 mol%) of Dy_2O_3 in the glasses or they selected only 1.0 mol% of Dy_2O_3 to study the glasses systems [15–18]. To crack this erratum, we in the present study employed co-dopant technique, which is used to overcome the quenching state and to enhance the sensitivity for dopant. The addition of a second modifier reagent enhances the emission intensity, creates disruption in the lattice, opens the network structure, weakens the bond strength, and lowers the viscosity of glass [19–21].

The present work focusses on the role of Dy_2O_3 in absence/presence of aluminium oxide by making comparative study of two glass systems Dy_2O_3–PbO–B_2O_3 (DY) and Dy_2O_3–Al_2O_3–PbO–B_2O_3(DYA). Also, the lasing properties have been discussed by absorption, photoluminescence, lifetime and CIE chromaticity color coordinates for different applications in solid state lighting field.

2. Experimental details

The detailed composition of various samples prepared for the present investigation has been tabulated below in Table 1

The raw materials dysprosium oxide (Dy_2O_3), lead oxide (PbO), boronoxide (B_2O_3) and aluminium oxide (Al_2O_3) in proper amounts are mixed and grinded finely to get a final batch of 15 g. The grinded mixture is further melted in silica crucible for 1 h in an electric furnace at a temperature of 1200^0 C in normal atmosphere till the formation of a bubble free liquid. Further, the melt has been quenched into preheated steel mould and annealed at a temperature of 400^0C. It is allowed to cool to room temperature to eliminate thermal and mechanical stress. The obtained samples are then grounded using different grade of SiC and polished with cerium oxide to have maximum flatness making them amenable for spectroscopic studies.

3. Characterisation

To confirm the amorphous/crystalline nature of the samples, X-ray diffraction (XRD) study has been done using XRD- 7000 Shimadzu X-ray Diffractometer (Cu Kα, λ = 1.54434 Å) at the rate of 2°/min with 2θ varying from 10° to 70°. The standard Archimede's principle is used to find the density of glass samples by using a sensitive microbalance with pure benzene as the immersion fluid.

$$D = [W_A/(W_A - W_B)]d, \quad (1)$$

where W_A is the weight of sample in air, W_B is the weight of the sample in benzene, and d is the density of the benzene. The molar volume (V_{im}) is calculated with the help of following formula:

$$V_{im} = \Sigma x_i M_i/d \quad (2)$$

where x_i is the molar fraction of the component and M_i is its molecular weight. The optical absorption spectra of the polished samples has been recorded at room temperature with the help of a (UV–Vis–NIR) Perkin Elmer Lambda 35 Spectrometer in the range 200–1100 nm with a spectral resolution of ± 1 nm. The optical band gap (E_g) has been calculated using the model proposed by Mott and Davis for indirect transitions observed in case of glasses due to long range geometrical disorder. The fluorescence spectra of prepared samples has been recorded with the help of Perkin-Elmer Fluorescence LS 45 Spectrophotometer with a resolution of ± 1.0 nm. The time-resolved fluorescence spectra have been recorded with a BH-CHRONOS time resolved fluorescence spectrophotometer using laser diodes at an excitation wavelength of 386 nm. The infrared transmission spectra of the samples are measured by using Varian 660-IR FTIR Spectrophotometer with spectral resolution of 4 cm^{-1} in the wavenumber range 400–4000 cm^{-1}. The fine powder of prepared glasses is mixed with KBr in the ratio 1:100 (glass powder: KBr) and a pressure of 1.470×10^7 Pa is applied to the mixture to get homogenous pellets. The IR transmission measurements are made instantly after preparing the pellets to avoid moisture.

Table 1
Nominal chemical composition of prepared glasses samples (mole %).

Sample Code	**xDy_2O_3–20PbO–(80-x)B_2O_3 and xDy_2O_3–(10-x) Al_2O_3–20PbO–70B_2O_3**			
	Dy_2O_3 (%)	Al_2O_3(%)	PbO (%)	B_2O_3 (%)
DY1	0.5	0	20	79.5
DY2	1.0	0	20	79
DY3	1.5	0	20	78.5
DY4	2.0	0	20	78
DYA1	0.5	9.5	20	70
DYA2	1.0	9.0	20	70
DYA3	1.5	8.5	20	70
DYA4	2.0	8.0	20	70

4. Experimental results and discussion

4.1. X-ray diffraction analysis

X-ray diffraction patterns of DY and DYA glass samples (Fig. 1) confirms absence of continuous or discrete sharp peaks but consist of diffused halos that reflects the glassy nature of the prepared samples. However, the diffractograms associated with alumino borates show a slight hint of crystallinity with very low intensity broad and diffused peaks [22].

4.2. FTIR spectra of Dy_2O_3–$PbO-B_2O_3$ glasses and Dy_2O_3–$Al_2O_3-PbO-B_2O_3$ glasses

4.2.1. Dy_2O_3–$PbO-B_2O_3$ glasses

The FTIR spectra of the prepared glass samples have been recorded at room temperature is shown Fig. 2(a & b) depicting the presence of

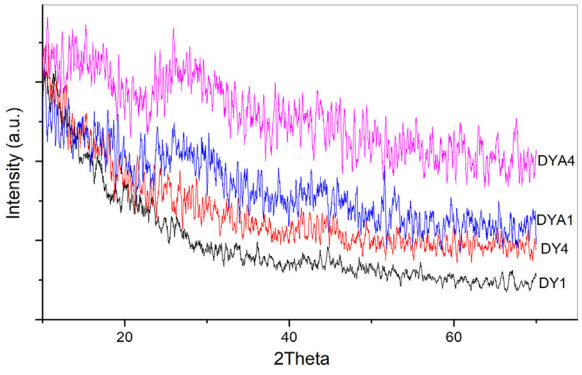

Fig. 1. XRD of DY and DYA prepared glass samples.

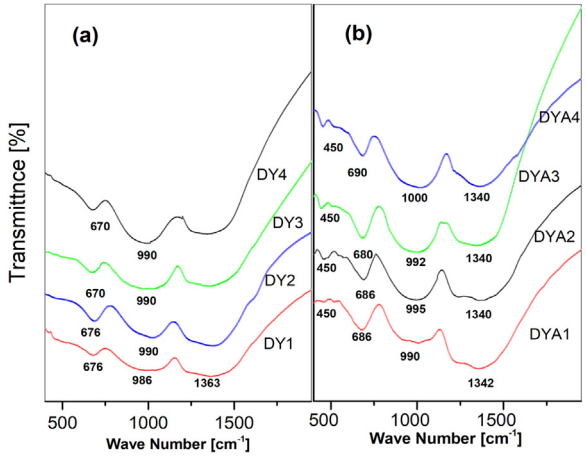

Fig. 2. (a & b) FTIR spectra of Dy_2O_3-PbO-B_2O_3 (DY) and Dy_2O_3-PbO- Al_2O_3-B_2O_3 (DYA) glasses as a function of Dy_2O_3 concentration ranging from 0.5% to 2%.

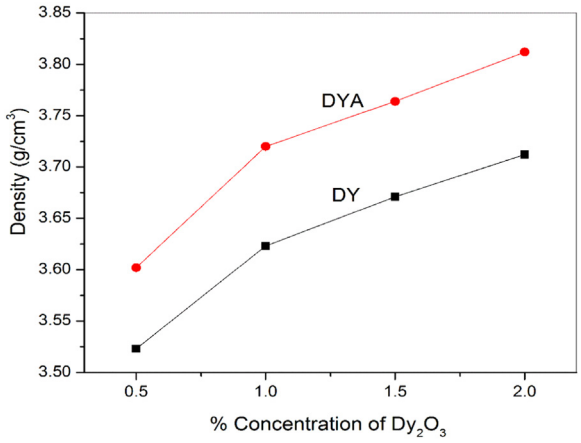

Fig. 3. Density of Dy_2O_3-PbO-B_2O_3 (DY) and Dy_2O_3-PbO- Al_2O_3- B_2O_3 (DYA) glasses as a function of Dy_2O_3 concentration ranging from 0.5% to 2%.

different structural groups along with the variations occurring in their arrangements with change in the glass composition. The FTIR spectra have been mainly divided into three regions: (i) 600–800 cm^{-1} is ascribed to bending vibrations of different B-O-B bonds, (ii) 800–1200 cm^{-1} is for stretching vibrations of BO_4 groups and (iii) 1200–1600 cm^{-1} presents the B-O stretching vibrations of BO_3 groups.

The absence of peak at 806 cm^{-1} indicates that no boroxol ring have been formed and the glass samples consist of BO_3 and BO_4 groups only [23]. The band at 676 cm^{-1} in the samples confirms the combined presence of BO_4 and PbO_4 groups [24]. The intensity of this band increases with increase in dysprosium content. The band at 986 cm^{-1} has been attributed to B-O bond stretching vibrations of BO_4 groups [25]. With addition of dysprosium oxide in borate network, the intensity of this band increases alongwith shifting towards higher wavenumber which may be attributed to stretching of B-O-M (B-O-Pb) linkage [26] and conversion of BO_3 to BO_4 groups [27]. The band at 1363 cm^{-1} has been associated with BO_3 groups stretching vibrations [28]. The shifting of this band with addition of dysprosium oxide may be due to asymmetric stretching of Dy-O-B (3) linkage [29] and pure B (3)–O–B (3) groups. The intensity of bands between 1200 and 1600 cm^{-1} shows a decreasing trend which depicts that trigonal BO_3 groups have been converted into tetrahedral BO_4 groups with increment of dysprosium concentration.

4.2.2. Dy_2O_3–Al_2O_3 – PbO – B_2O_3 glasses

In this glass composition, the band at 686 cm^{-1} have higher intensity and broadness than the same ban at 676 cm^{-1} in the Dy_2O_3-PbO-B_2O_3 glasses. This band consists of combined vibration of B-O-B and AlO_4 groups [30–32]. The band at 990 cm^{-1} in DYA1 sample is due to B-O bond stretching vibrations of BO_4 groups [33]. This band shifts towards higher wavenumber and show an increase in intensity with increase in dysprosium content. Since the aluminium and borate groups share the same position, the increase in intensity and shifting of this band may be assigned to the joint presence of (AlO_4) groups of aluminium and BO_4 units. [28–32]. The band at 1342 cm^{-1} has been attributed to BO_3 groups [34]. Another band at 450 cm^{-1} in the sample DYA2 has been assigned to the combined presence of AlO_6 groups and dysprosium ions' vibrations at the network sites [35–40], forming Dy-O-Al bond [41]. The shifting of this band indicates that dysprosium tends to form such more groups by providing more oxygen to aluminium.

From the above discussion, it may be concluded that dysprosium plays the role of modifier in both the glass systems, but dysprosium oxide modifies DYA glass system in a better way by converting more BO_3 to BO_4 groups. Besides dysprosium oxide, addition of alumina at low concentration in borate glasses modifies the network structural units by converting BO_3 to BO_4 groups [42,43].

4.3. Density and physical properties

Density measurement is a potent tool for inquiring the changes incurred in the glass structure due to compositional variations subsequently as these are affected by the change in coordination number and structural compaction on the addition of various modifiers [44]. The density of synthesized glasses increases with the substitution of aluminium and dysprosium as shown in Fig. 3. From Tables 2 and 3, it can be confirmed that the aluminate glasses possess higher density as compared to non-aluminate glasses. This can be explained on the basis of structural changes occurring in coordination of boron in glass network as in the presence of Al_2O_3 a large number of oxygen ions are accessible in glass structure. These oxygen ions aid to convert three coordinated boron units BO_3 to four coordinate boron units (BO_4) which are considerably denser than the symmetric BO_3 trigonals [45].

From Tables 2 and 3 it has been observed that molar volume decreases with Dy_2O_3 content which reflects reduction in bond length or interatomic spacing between the atoms. The compaction of glasses, the average boron–boron separation d_b-d_b [46] and interionic separation (r_i) have been confirmed and calculated [47] using Eq. (3) as given below.

$$V_M^B = \frac{V_B}{2(1-X_B)} \tag{3}$$

where V_m is the molar volume and X_B the molar fraction of B_2O_3:

Table 2
Different physical and optical parameters of in Dy_2O_3-PbO-B_2O_3 (DY) as function of Dy_2O_3 ranging from 0.5% to 2%.

Physical and Optical Parameters	Glass Sample			
	DY1	DY2	DY3	DY4
Density (g/cm^3)	3.523	3.623	3.69	3.76
Molar volume (cm^3/vol.)	28.909	28.529	28.422	28.297
Boron-Boron separation: $d_{<B-B>}$ (nm)	0.4892	0.4831	0.4788	0.474
Molar volume of Oxgyen: V_0 (cm^3/vol.)	11.12	10.97	10.93	10.88
Electronegativity Difference: $\Delta\chi$	1.3461	1.3502	1.3543	1.3584
Optical band gap (eV)	2.89			2.87
Number of ions: N × 10^{20} (ions/cm^3)	2.083	4.222	6.357	8.514
Interionic distance (Å)	16.86	13.33	11.63	10.55
Polaron radius (Å)	6.799	5.372	4.686	4.252

Table 3
Different physical and optical parameters of Dy_2O_3-PbO- Al_2O_3- B_2O_3 (DYA) as function of Dy_2O_3 ranging from 0.5% to 2%.

Physical and Optical Parameters	Glass Sample			
	DYA1	DYA2	DYA3	DY4
Density (g/cm^3)	3.602	3.72	3.78	3.85
Molar volume (cm^3/vol.)	29.129	28.569	28.474	28.308
Boron-Boron separation: d $_{<B-B>}$ (nm)	0.432	0.429	0.428	0.427
Molar volume of Oxgyen: V_0 (cm^3/vol.)	11.203	10.988	10.952	10.889
Electrnegativity Difference: $\Delta\chi$	1.386	1.389	1.391	1.393
Optical band gap (eV)	2.81			2.80
Optical Basicity: (OB)	0.5351	0.5371	0.5391	0.541
Number of ions: N × 10^{20} (ions/cm^3)	2.067	4.216	6.346	8.511
Interionic distance (Å)	16.911	13.336	11.637	10.552
Polaron radius (Å)	6.816	5.375	4.690	4.253

$$<d_{b-b} \geq \left(\frac{V_M^B}{N_A}\right)^{\frac{1}{3}} \quad (4)$$

The results shown in Tables (2 and 3) show a gradual decrease in the average boron–boron separation resulting in decreased affinity for expansion of the glass network. But this effect is more prominent in glasses containing Al_2O_3 which again confirms the densification of both glass systems.

Further molar volume of oxygen (V_o) and oxygen packing density (OPD) have been calculated using the following formula [48,49]

$$V_o = \sum_i \frac{V_m}{x_i n_i} \quad (5)$$

$$OPD = 1000C\left(\frac{\rho}{M}\right) \quad (6)$$

From the Tables 2 and 3 it is confirmed that both V_0 and OPD shows an opposite relationship (V_0 decreases and OPD increases). This behavior reveals the fading of non-bridging oxygen and formation of bridging oxygen with the incorporation of Dy_2O_3 leading to more compact glass structure.

4.4. UV–Vis spectroscopy of Dy_2O_3–PbO–B_2O_3 (DY) and Dy_2O_3–Al_2O_3–PbO–B_2O_3 (DYA) glasses

The optical absorption spectra of DY1 and DYA1, DY4 and DYA4 have been shown in Fig. 4 The glass system without aluminium shows the optical absorption edge at around 396 nm in DY1 and DY4 respectively. Whereas in the presence of aluminium absorption edge shows a noticeable red shift from 396 to 417 nm for the same concentration of dysprosium. The absorption spectra of Dy^{3+} ions consist of twelve inhomogeneously broadened transitions from the $^6H_{15/2}$ ground state to the $^6P_{7/2}$ at 365 nm, $^4F_{7/2}$ and $^4I_{13/2}$ at 386 nm, $^4G_{11/2}$ at 425 nm, $^4I_{15/2}$ at 449 nm, $^4G_{9/2}$ at 472 nm, $^6F_{3/2}$ at 752 nm, $^6F_{5/2}$ at 802 nm, $^6F_{7/2}$ at 900 nm, $^6F_{9/2}$ + $^6H_{7/2}$ at 1092 nm, $^6F_{11/2}$ + $^6H_{9/2}$ at 1271 nm, $^6H_{11/2}$ at 1683 nm and $^6H_{13/2}$ at 2180 nm belonging to the $4f^9$ electronic configuration. The absorption band positions for the Dy^{3+} ions doped glasses fall almost at the same positions regardless of the variation in chemical composition, though there is only a change in intensity of the different bands. These observations clearly indicate an increase in the cut off wavelength thus causing a red shift with dysprosium oxide content. The oxygen bonding in glass forming network changes significantly in glasses containing aluminium than those without it, because the position of absorption edge depends on the oxygen bond strength in the glass forming network [50]. The above details are also in agreement with density and FTIR results. Hence confirming the presence of more BO_4 groups in DYA glasses which are responsible for a comparatively smaller band gap as compared to those of DY glasses. Since the presence of small amount of Al_2O_3 (less than 10%) [13] helps in converting trigonal BO_3 to more tetrahedral BO_4 groups.

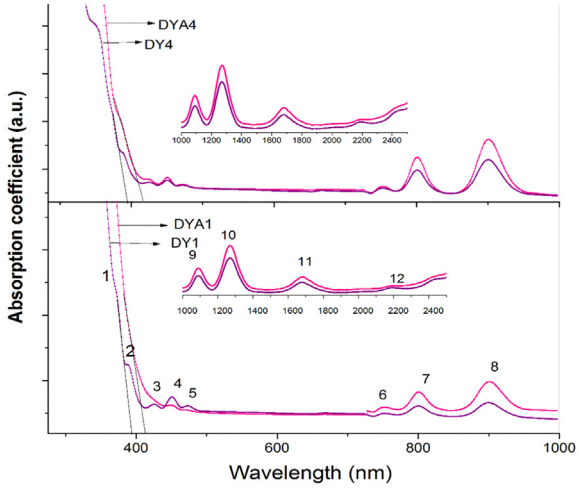

Fig. 4. Optical absorption spectra of PbO-Dy_2O_3-B_2O_3 (DY1 & DY4) and Dy_2O_3-PbO- Al_2O_3- B_2O_3 (DYA1 & DYA4) glasses.

4.5. Excitation and Luminescence spectra of Dy_2O_3– PbO–B_2O_3 (DY) and Dy_2O_3–Al_2O_3–PbO–B_2O_3 (DYA) glasses

The excitation spectrum presented in Fig. 5 of DY4 and DYA4 has been monitored at λ_{em} = 574 nm ($^4F_{9/2}$ →$^6H_{13/2}$ transition) in 300–500 nm spectral range. Numerous constricted bands belonging to the well-known high lying f–f electronic transitions of Dy^{3+} ions are observed. Any broad excitation charge-transfer bands due to Dy^{3+}–O^{2-} interactions have not been obtained in the short wavelength spectral region. The observed bands are assigned to transitions originating from the $^6H_{15/2}$ ground state to the $^4F_{9/2}$ at 474 nm, $^4I_{15/2}$ at 451 nm, $^4G_{11/2}$ at 425 nm, $^4I_{13/2}$ + $^4F_{7/2}$ + $^4K_{17/2}$ at 387 nm, and (^4M + $^4I)_{15/2}$ at 357 nm states of Dy^{3+} ions. Out of these the transitions at 387 nm and 451 nm are the most intense.

The emission spectra of Dy_2O_3-PbO-B_2O_3 (DY) and Dy_2O_3-Al_2O_3-PbO-B_2O_3 (DYA) glasses excited at 386 nm show blue, yellow and red emissions between 6 F and 6 H levels of Dy^{3+} ions shown in Fig. 6(a & b). The λ_{exc} = 386 nm excites the Dy^{3+} ions to the hypersensitive level $^6P_{7/2}$, from where they relax non-radiatively to the $^4F_{9/2}$ metastable level. The emission spectra of DY and DYA glasses consist of mainly three peaks. These transitions correspond to $^6H_{15/2}$, $^6H_{13/2}$ and $^6H_{11/2}$ to ground state ($^4F_{9/2}$) of Dy^{3+} ions. These three visible emissions along with excitation wavelength are shown in the energy level diagram in Fig. 7. Due to small energy gaps between all states lying above

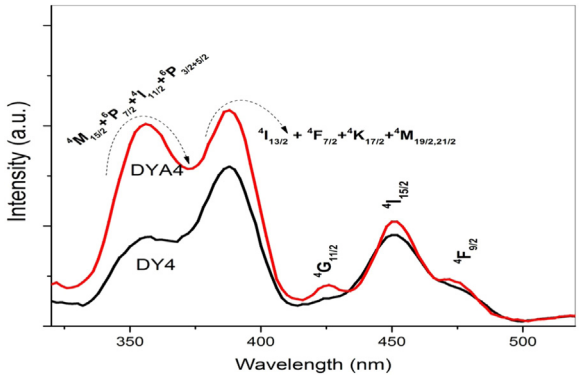

Fig. 5. Excitation spectra of Dy_2O_3– PbO–B_2O_3 (DY4) and Dy_2O_3–Al_2O_3–PbO–B_2O_3 (DYA4) glasses at λ_{em} = 565 nm.

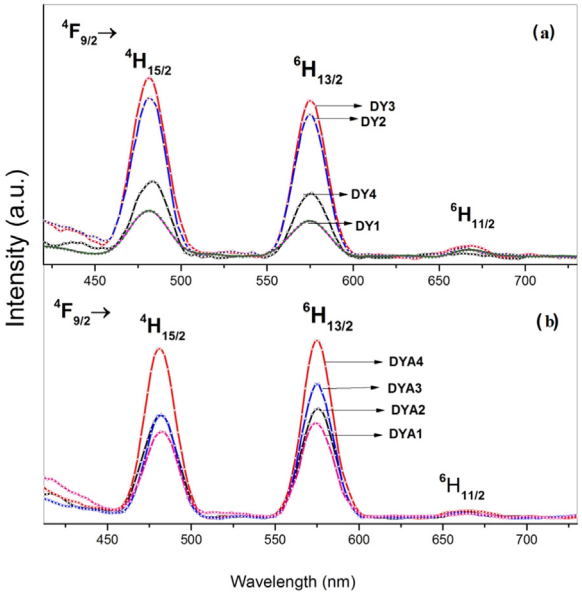

Fig. 6. (a & b). Emission spectra of Dy_2O_3-PbO-B_2O_3 (DY) and Dy_2O_3-PbO-Al_2O_3- B_2O_3 (DYA) glasses as a function of Dy_2O_3 concentration ranging from 0.5% to 2% excited at 386 nm.

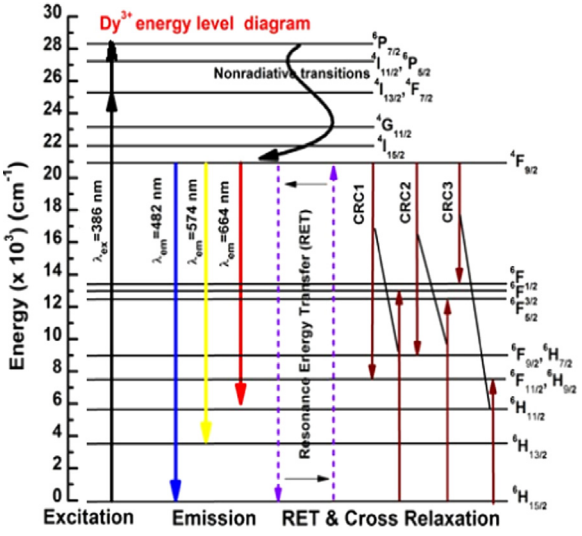

Fig. 7. Energy level diagram of Dy^{3+} ions demonstrating excitation, emission and energy transfer mechanisms.

21,000 cm^{-1}, the $^4F_{9/2}$ state is well populated by non-radiative relaxation. A quite strong yellow/blue luminescence due to $^4F_{9/2}$→ $^6H_{J/2}$ (J = 13, 15) transitions is observed which is related to large separation (~6000 cm^{-1}) between $^4F_{9/2}$ state and $^6F_{1/2}$ state and the relative high phonon energy of the host (~1300 cm^{-1}).

The emission spectra shown in Fig. 6(a) consists of two main bands. One at 480 nm (blue) which corresponds to the magnetic dipole (MD) transition which hardly varies with the crystal field around Dy^{3+} ions and corresponds to the $^4F_{9/2}$→$^6H_{15/2}$ transition. Another band at 572 nm (yellow) corresponding to $^4F_{9/2}$→$^6H_{13/2}$ transition is hypersensitive transition (forced dielectric dipole ED) with the selection rule ($|\Delta L| \leq 2$ and $\Delta J| \leq 2$) which is strongly influenced by the environment. A third very weak band at 663 nm (red) has also been observed which is due to $^4F_{9/2}$→$^6H_{15/2}$ transition. The fluorescence intensity in DY glass samples increases with dysprosium concentration and attains maximum intensity at 1 mol% but above 1 mol% concentration of Dy^{3+}ions, the intensity decreases resulting in luminescence quenching. Two main mechanisms which may be employed to explain this concentration quenching are resonance energy transfer (RET) and cross relaxations (among neighboring Dy^{3+} ions) between two closely located rare earth ions due to the tendency of Dy^{3+} ions to form clusters through Dy—O—Dy bonds. In cross relaxation mechanism, an excited Dy^{3+} ion drops some portion of its excitation energy to a neighboring Dy^{3+} ion at the ground state and stimulates it to some intermediate states. Thus, both participating Dy^{3+} ions goes to metastable state. In view of the energy resonance [51,52], three cross relaxation channels (CRC) can be identified:

CRC1: $^4F_{9/2} + {}^6H_{15/2} \rightarrow ({}^6H_{9/2} + {}^6F_{11/2}) + {}^6F_{5/2}$
CRC2: $^4F_{9/2} + {}^6H_{15/2} \rightarrow ({}^6H_{7/2} + {}^6F_{9/2}) + {}^6F_{3/2}$
CRC3: $^4F_{9/2} + {}^6H_{15/2} \rightarrow {}^6F_{1/2} + ({}^6H_{9/2} + {}^6F_{11/2})$

Fig. 6(b) shows emission spectral profile of DYA series with three peaks at 482, 573 and 667 nm. There is a continuous increase in the luminescence intensity from DYA1 to DYA4 with no quenching of luminescence.

4.5.1. *Hypersensitive transition*

Dy^{3+} ions work as spectroscopic probe for local structure due to electric dipole character of $^4F_{9/2}$→$^6H_{13/2}$ hypersensitive transition, whose intensity increases as it is very sensitive to crystal field. It has been used to measure the degree of symmetry of the local environment of trivalent 4f ions. Fig. 8 clearly shows an inverse relation between the intensity of ED transition and the environmental symmetry of luminescence site. The intensity ratio of ED to MD transitions also called yellow/blue ratio have been calculated. It is further noted that there is a significant change in the relative emission intensities with change in the concentration of Dy^{3+} ions and host environment (addition of aluminium). These changes are quantified as Y/B intensity ratios and are presented in Table 5. The Y/B ratio portrays the site symmetry and the electronegativity of the surrounding ligands of rare earth ions site [53]. It is observed from the results depicted in Fig. 8 that the presence of aluminium intensifies the $^4F_{9/2}$ →$^6H_{13/2}$ (ED) transition over $^4F_{9/2}$ →$^6H_{15/2}$ (MD) emission transition. It is found that Y/B ratio of non-aluminate glasses increases upto 1.0 mol% of Dy^{3+} ion content and beyond that it decreases due to the change in symmetry around the Dy^{3+} ion site. This indicates that the Dy^{3+} ions are present at the higher symmetry site (with the inversion symmetry) in aluminate glasses confirming the higher covalent interaction between $O^{2-}$and Dy^{3+} ions [54].

Thus, the addition of modifiers i.e.; Al_2O_3 or PbO in the glasses results in declusterization of Dy^{3+} ions which effects the fluorescence of DYA samples and the intensity of the hypersensitive emission at

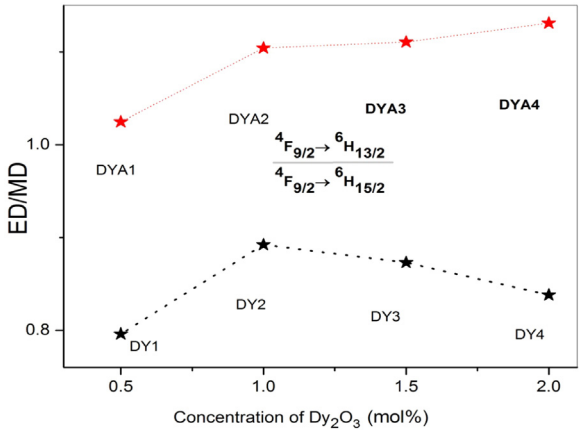

Fig. 8. Electric to Magnetic dipole transition ratio of Dy_2O_3-PbO-B_2O_3 (DY) and Dy_2O_3-PbO- Al_2O_3- B_2O_3 (DYA) as function of Dy_2O_3 ranging from 0.5% to 2%.

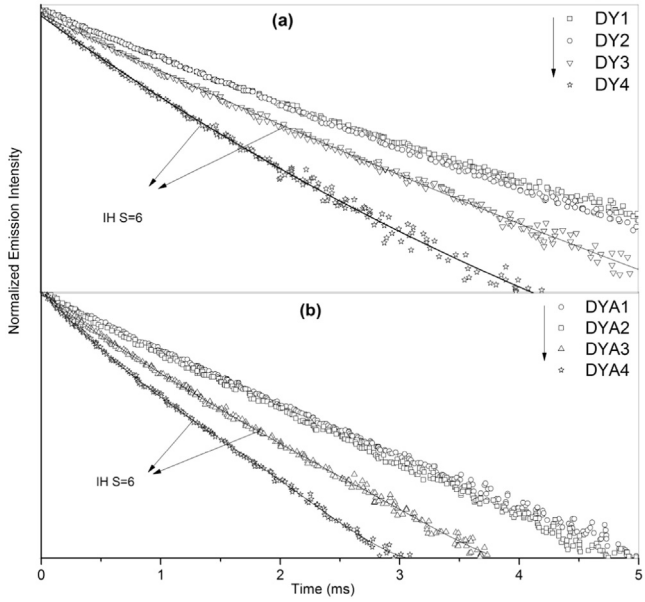

Fig. 9. The decay profiles for the $^4F_{9/2}$ excited of Dy^{3+} ions in Dy_2O_3-PbO-B_2O_3 (DY) and Dy_2O_3-PbO- Al_2O_3- B_2O_3 (DYA) as function of Dy_2O_3 ranging from 0.5% to 2%.

575 nm (yellow region). Addition of Al_2O_3 to the glasses modifies the vicinity of dysprosium ions by transforming glass network and rearranging BO_3 and BO_4 units to new positions. Addition of Al_2O_3 enhances the covalency due to overlapping of oxygen orbitals with 5d orbitals of dysprosium leading to accommodation of aluminium groups in the network of BO_4 tetrahedra around Dy^{3+} ions. As depicted in IR spectra, incorporation of Al_2O_3 increases BO_4 groups which results in increasing Dy-O bond covalency due to more asymmetry resulting in the increased luminescence. Thus, aluminium by playing the dual role as a modifier and a former increases the solubility of Dy^{3+} ion clusters in the host glass system [55,56] thus enhancing photoluminescence.

4.6. Decay analysis

Fig. 9 represents decay curves of the intense luminescent $^4F_{9/2} \rightarrow {}^6H_{13/2}$ transition of Dy^{3+} ions. It has been observed that the samples with lesser Dy^{3+} ion concentration (0.1 mol%) follow single exponential function but deviates to non-exponential nature for higher Dy^{3+} ion concentrations (≥ 0.5 mol%). The non-exponential nature of the decay curves at higher concentrations of the rare earth generally comes from ion–ion interactions. It can be explained clearly on the basis of resonant energy transfer between Dy^{3+} ions and are fitted well to Inakuti–Hirayama (IH) model [57] for S = 6, indicating that the energy transfer between the Dy^{3+} ions is due to dipole–dipole interactions. The IH model expression is given as below (Eq. (7)):

$$I(t) = I_0 \exp\{-\frac{t}{t_0} - Q\left(\frac{t}{t_o}\right)^{\frac{3}{S}}\} \quad (7)$$

The energy transfer parameter 'Q', donor–acceptor interaction parameter (C_{DA}) and the critical distance (R_0) between donor and acceptor can be obtained from the non-exponential decay curves using the relation (Eq. (8)):

$$Q = \frac{4\pi}{3}\Gamma\left(1-\frac{3}{S}\right)N_0 R_0^3 \quad (8)$$

where the Γ function, Γ(x), is equal to 1.77 in the case of dipole–dipole interaction (S = 6), 1.43 for dipole– quadrupole interaction (S = 8) and 1.3 for quadrupole–quadrupole interaction (S = 10). N_0 is the concentration of acceptors, which is equal to the concentration of RE^{3+} ions and R_0 is the critical transfer distance defined as the donor–-acceptor separation for which the rate of energy transfer to the acceptors is equal to the rate of intrinsic decay of the donors. The donor–acceptor coupling constant (C_{DA}) is given by (Eq. (9)):

$$C_{DA} = \frac{R_0^6}{\tau_0} \quad (9)$$

Table 4
Experimental lifetime (lifetime, μs), energy transfer parameters (Q), critical transfer distances (R_o nm) and donor-acceptor coupling constants (C_{DA} x10^{42} cm^6 /s) for various concentrations of Dy^{3+} ions in prepared glasses.

S.No.	τ_{exp} (μs)	Q	R_o (nm)	C_{DA} × 10^{40} (cm^6/s)
DY1	598	–	–	–
DY2	515	–	–	–
DY3	321	0.61	7.3	1.14
DY4	247	1.06	9.48	6.8
DYA1	617	–		
DYA2	589	–		
DYA3	470	0.55	6.7	1.01
DYA4	387	0.96	7.2	3.30

The values of Q, Ro and the donor–acceptor interaction parameter (C_{DA}) are presented in Table 4. The lifetimes have been found to decrease with increase in C_{DA} values. This clearly indicates that the energy transfer by dipole–dipole interaction between the two Dy^{3+} ions is the major cause for the lifetime quenching in the present glass system and is responsible for non-exponential behavior of decay curves. The energy transfer by the dipole–dipole interaction mainly prevails among the various mechanisms in glasses doped with rare earths [58–60].

With increase in the dysprosium concentration the fluorescence lifetime of $^4F_{9/2}$ level of these glasses in the presence and absence of aluminium decreases from 617 to 387 μs and 598–247 μs respectively, and are presented in Table 4. The $^4F_{9/2}$ luminescence lifetime of aluminate glasses is slightly on the higher side as compared to non-aluminate glasses. The addition of Al_2O_3 helps in de-polymerization of the repeating glassy matrix, leading to a change in the coordination environment of the cations in the vicinity of the RE ions.

4.7. White light emission and Colorimetery

The emission intensities have been characterized by calculating chromaticity color coordinates using the CIE 1931 chromaticity diagram shown in Fig. 10. The calculated chromaticity coordinates for the present glass system appeared in the white light region of the CIE 1931

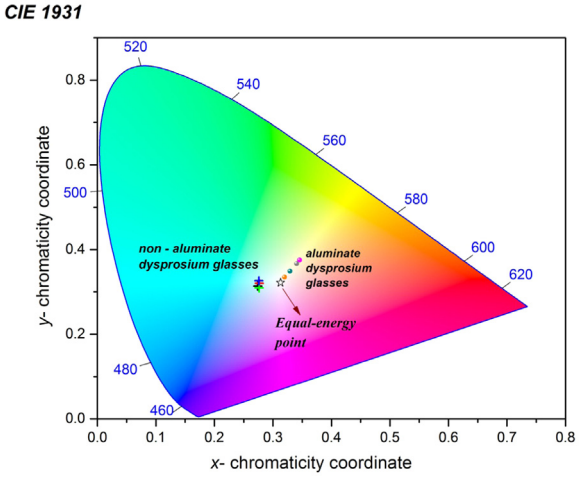

Fig. 10. The chromaticity diagram of the emissions observed in the glass samples Dy_2O_3 -PbO- B_2O_3 (DY) and Dy_2O_3-PbO- Al_2O_3- B_2O_3 (DYA) excited at 386 nm.

Table 5
The yellow-blue ratios, CIE color co-ordinates (x,y), CCT and color purity for Dy^{3+} ions in all the glasses.

S.No.	Y/B	Color coordinates	CCT (K)	Color Purity
DY1	0.838	0.284, 0.312	7869	0.148
DY2	0.873	0.286, 0.320	7572	0.133
DY3	0.892	0.283, 0.309	7979	0.157
DY4	0.796	0.286, 0.325	7514	0.130
DYA1	1.131	0.345, 0.375	5052	0.179
DYA2	1.110	0.340, 0.367	5217	0.129
DYA3	1.104	0.329, 0.348	5633	0.0447
DYA4	1.024	0.3199, 0.335	6095	0.034

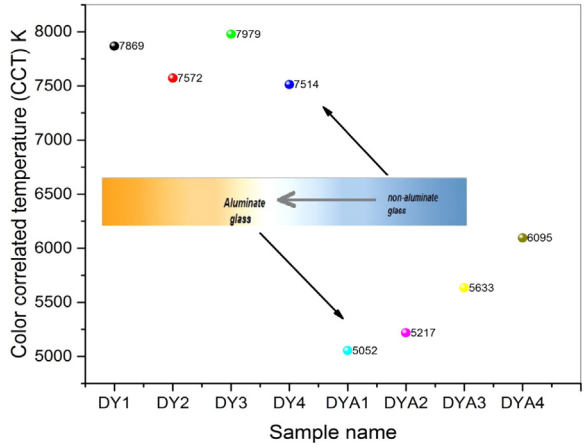

Fig. 11. CCT of the glass samples Dy_2O_3 -PbO- B_2O_3 (DY) and Dy_2O_3-PbO-Al_2O_3- B_2O_3 (DYA) excited at 386 nm.

chromaticity diagram. The chromaticity coordinates of samples without aluminium lie closer to CIE standard D65 illuminant (x = 0.31, y = 0.33) while the samples with aluminium (especially DA3 and DA4) lie very close to standard equal energy white illuminant (x = 0.33, y = 0.33). Hence suggesting these glasses to be potential candidate for the generation of white light (average daylight illuminant) by using commercial UV LED chip (under excitation λ_{ex} = 386 nm) [61].

White color may further be trimmed from two dimensions to just one, with the concept of Correlated Color Temperature (CCT). The color temperature of a light source is the temperature of the Planckian's black body radiator, whose radiation has the same chromaticity as the light source. CCT is an important parameter to characterize a vital feature about illuminants, like, their role on our emotional state, mental well-being and visual acuity. Many researchers have established that cool white light (high CCT or high blue content) results in an increase in visual activity and concentration. Therefore, cool white lights are preferred for lighting in schools, offices, hospitals etc. Although on the other hand, a warmer light (low CCT) be likely to be employed more prominently in houses, restaurants, hotels etc., where the warmer light offers a calm, peaceful and relaxed atmosphere [62,63]. The CCT of various glass samples has been calculated from the chromaticity co-ordinates which is applied between 2222 K and 13,000 K. This relation is given by the McCamy's relation [64] as given below

$$CCT(x, y) = -449n^3 + 3525n^2 - 6823.3n + 5520.33 \quad (10)$$

Where n is given by n = (x—0.3320)/(y—0.1858)

The CCT values, color coordinates and Y/B values of the prepared glasses are presented in Table 5. The glasses containing aluminium exhibit lower CCT values as compared to non-aluminate glasses. So, the presence of aluminium shifts CCT values towards warm white color (5500 K) from cool white color (near 6400 K) resulting in the use of these glasses for warm white light applications as shown in Fig. 11. The color purity or color saturation is another important tool to understand better about the light sources for LED applications. It is the distance in the chromaticity diagram between the (x, y) color-coordinate point of the test source and the coordinate of the equal-energy point divided by the distance between the equal-energy point and the dominant-wavelength point. The color purity is thus given by (eq. (11)) [65]

$$colorpurity = \frac{Distance\ between\ the\ coordinates\ of\ the\ respective\ glass\ and\ equal\ energy\ point}{Distance\ between\ equal\ energy\ point\ and\ dominant\ wavelength\ point} \quad (11)$$

Dominant wavelength for a source is the wavelength at which a straight line passing through the equal energy point and co-ordinates of the source meet the perimeter of the chromaticity diagram. The color purity for the standard white light is 0%, so it should be as low as possible to accomplish white light emission from the emitting sources. The color purity calculated for different glass samples has been presented in Table 5. The low color purity of the synthesized samples at low aluminium concentration is clearly indicated which makes these glasses suitable for the generation of white light.

5. Conclusion

1. In DYA glasses aluminium unsystematically distributes around Dy^{3+} ions and forms a relatively low symmetry environment around the dysprosium ions. The improvement of emission after co-doping aluminium with dysprosium clearly shows that aluminium ions modify the local environment around Dy^{3+} ions and strongly antiquenches photoluminescence.
2. The CIE color chromaticity coordinates of the prepared glasses have been tuned for white light emission by varying the Dy^{3+} ion concentration as well as the host matrix environment and are found to be close to the standard values (0.33, 0.33). Since the calculated CIE color coordinates, CCT and color purity values of DA3 and DA4 glass samples are in good agreement with the daylight and commercial WLEDs.
3. Fluorescence decay rates of the $^4F_{9/2}$ level of Dy^{3+} ions change from single exponential to non-exponential nature associated with quenching of lifetimes with increase in Dy^{3+} ion's concentration due to enhancement of energy transfer processes between Dy^{3+} ions.
4. Dysprosium oxide modifies the Dy_2O_3–Al_2O_3–PbO–B_2O_3 glass system comparatively in a better way by converting more BO_3 groups to BO_4 groups with addition of alumina at low concentration.

References

[1] A. Agnesi, P. Dallocchio, F. Pirzio, G. Reali, Opt. Commun. 282 (2009) 2070.
[2] H. Kalaycioglu, H. Cankaya, G. Ozen, L. Ovecoglu, A. Sennaroglu, Opt. Commun. 281 (2008) 6056.
[3] I. Iparraguirre, J. Azkargorta, J.M. Fernandez-Navarro, M. Al-Saleh, J. Fernandez, R. Balda, J. Non- Cryst. Solids 353 (2007) 990.
[4] J.C. Zhang, C. Parent, G. le Flem, P. Hagenmuller, J. Solid State Chem. 93 (1991) 17.
[5] S. Liu, X. Li, X. Yu, Z. Chang, P. Che, J. Zhou, W. Li, J. Alloy. Compd. 655 (2016) 203–207.
[6] M. Zhang, Y. Liang, S. Xu, Y. Zhu, X. Wu, S. Liu, CrystEngComm 18 (2016) 68.
[7] P. Pawar, S. Munishwar, R. Gedam, J. Alloy. Compd. 660 (2016) 347–355.
[8] T. Leow, H. Liu, R. Hussin, Z. Ibrahim, K. Deraman, H. Lintang, W. Shamsuri, J. Rare Earths 34 (2016) 21–29.
[9] Y.W. Seo, S.H. Park, S.H. Chang, J.H. Jeong, K.H. Kim, J.-S. Bae, Ceram. Int. 43 (2017) 8497–8501.
[10] G.A. Kumar, A. Martinez, E. Mejia, J.G. Eden, J. Alloy. Compd. 365 (2004) 117.
[11] E. Culea, L. Pop, S. Simon, Mater. Sci. Eng. B 112 (2004) 59.
[12] K.S.V. Sudhakar, M. Srinivasa Reddy, L. Srinivasa Rao, N. Veeraiah, J. Lumin. 128 (2008) 1791.
[13] L. Srinivasa Rao, M. Srinivasa Reddy, M.V. Ramana Reddy, N. Veeraiah, Physica B 403 (2008) 2542.
[14] I.V. Kityk, W. Imio"ek, A. Majchrowski, E. Michalski, Opt. Commun. 219 (2003) 421.
[15] J. Kaewkhao, N. Wantana, S. Kaewjaeng, S. Kothan, H.J. Kim, J. Rare Earth 34 (2016) 583e589.
[16] L. Shamshad, G. Rooh, K. Kirdsiri, N. Srisittipokakun, B. Damdee, H.J. Kim, J. Kaewkhao, J. Alloy. Compd. 695 (2017) 2347e2355.
[17] A. Balakrishna, D. Rajesh, Y.C. Ratnakaram, J. Lumin. 132 (2012) 2984e2991.
[18] J.S. Kumar, K. Pavani, A.M. Babu, G.N. Kumar, S.B. Rai, L.R. Moorthy, J. Lumin.

130 (2010) 1916e1923.
[19] L. Jiang, Y. Zhang, C. Li, J. Hao, Q. Su, Appl. Radiat. Isot. 68 (1) (2010) 196–200.
[20] Y.S.M. Alajerami, S. Hashim, S.K. Ghoshal, A.T. Ramli, M.A. Saleh, Z. Ibrahim, D.A. Bradley, Appl. Radiat. Isot. 82 (2013) 12–19.
[21] S. Hashim, Y. Alajerami, S. Ghoshal, M. Saleh, M. Saripan, A. Kadir, Radiat. Phys. Chem. 104 (2014) 36–39.
[22] S. Kaur, G. Pal Singh, P. Kaur, D.P. Singh, J. Lumin. 143 (2013) 31.
[23] F.L. Galeener, G. Lucovsky, J.C. Mikkelsen Jr., Phys. Rev. B 22 (1980) 3983.
[24] H.M. Heaton, H. Moore, J. Soc. Glass Technol. 41 (1957) 28T.
[25] M. Arora, S. Baccaro, G. Sharma, D. Singh, K.S. Thind, D.P. Singh, NIM B 267 (2009) 817.
[26] A.A. Alemi, H. Sedghi, A.R. Mirmohseni, V. Golsanamlu, Radiat. Eff. Defects Solids 162 (2007) 351.
[27] G. Pal Singh, S. Kaur, P. Kaur, D.P. Singh, S. Kumar, D.P. Singh, Physica B 406 (2011) 1890.
[28] B. Karthikeyan, S. Mohan, Physica B 334 (2003) 298.
[29] G. El-Damrawi, K. El-Egilli, Physica B 229 (2001) 180.
[30] M. Handke, W. Mozgawa, M. Nocun, J. Mol. Struct. 325 (1994) 129.
[31] L. Stoch, M. Sroda, J. Mol. Struct. 511–512 (1999) 77.
[32] R.K. Brow, D.R. Tallant, J. Non-Cryst. Solids 222 (1997) 396.
[33] G. Pal Singh, P. Kaur, S. Kaur, D.P. Singh, Physica B 406 (2011) 4652.
[34] Yasser B. Saddeek, A.M. Abousehly, Shaban I. Hussien, J. Phys. D: Appl. Phys. 40 (2007) 4674.
[35] F. Moreau, A. Duran, F. Munoz, J. Euro, Ceram. Soc. 29 (2009) 1895.
[36] S.V.G.V.A. Prasad, M. Srinivasa Reddy, N. Veeraiah, J. Phys. Chem. Solids 67 (2006) 2478.
[37] A. Belkebir, J. Rocha, A.P. Esculcas, P. Berthet, B. Gilbert, Z. Gabelica, Spectro-Chim. Acta A 55 (1999) 1323.
[38] M.J. Weber, J. Non-Cryst. Solids 12 (1990) 208.
[39] E.I. Kamitsos, A.P. Patsis, M.A. Karakassides, G.D. Chryssikos, J. Non-Cryst. Solids 126 (1990) 52.
[40] C.A. Hogarth, M.N. Khan, J. Non-Cryst. Solids 123 (1990) 339.
[41] S.L. lin, C.S. Hwang, J. Non-Cryst. Solids 202 (1996) 61.
[42] R.L. Dhiman, V.S. Kundu, A.S. Maan, D.R. Goyal, J. Optoelec, Adv. Mater. 11 (2009) 1002.
[43] J.E. Shelby, Introduction to Glass Science and Technology, The Royal Society of Chemistry, Cambridge, UK, 1997.
[44] D. Singh, K. Singh, G. Singh, Manupriya, S. Mohan, M. Arora, G. Sharma, J. Phys.: Condens. Matter 20 (2008) 075228 (6pp).
[45] S. Rada, P. Pascuta, M. Culea, V. Maties, M. Rada, M. Barlea, E. Culea, J. Mol. Struct. 924–926 (2009) 89.
[46] Frank Berkemeier, Stephan Voss, Arpard W. Imre, Helmut Mehrer, J. Non-Cryst. Solids 351 (2005) 3816.
[47] A.S. Rao, Y.N. Ahammed, R.R. Reddy, T.V.R. Rao, Opt. Mater. 10 (1998) 245.
[48] S. Kaur, P. Kaur, G. Pal Singh, D. Arora, S. Kumar, D.P. Singh, J. Lumen. 180 (2016) 190–197.
[49] S. Kaur, P. Kaur, G. Pal Singh, S. Kumar, D.P. Singh, J. Opt. Mater. 47 (2015) 276–284.
[50] B.D. Mcswain, N.F. Borrel, S.V. Gongjen, Phys. Chem. Glasses 4 (1963) 1.
[51] Q. Su, J. Lin, B. Li, J. Alloy. Compd. 225 (1995) 120.
[52] S. Dutta, S. Som, S.K. Sharma, Dalton Trans. 42 (2013) 9654.
[53] Xingya Wu, Yujun Liang, Shiqi Liu, Yingli Zhu, Rui Xu, Miaohui Tong, Kai Li, Spectrosc. Lett. (2017), http://dx.doi.org/10.1080/00387010.2017.1287090.
[54] I. Arul Rayappan, K. Maheshvaran, S. Surendra Babu, K. Marimuthu, Phys. Status Solidi A 209 (3) (2012) 570–578.
[55] T. Satyanarayana, T. Kalpana, V. Ravi Kumar, N. Veeraiah, J. Lumin. 130 (2010) 498.
[56] Ni Yaru, Lu Chunhua, Zhang Yan, Zhang Qitu, Xu Zhongzi, J. Rare Earths 25 (2007) 94.
[57] M. Inokuti, F. Hirayama, Influence of energy transfer by the exchange mechanism on donor luminescence, J. Chem. Phys. 43 (1965) 1978–1989.
[58] R. Reisfeld, C.K. Jorgensen, in: K.A. Gschneidner Jr., L. Eyring (Eds.), Handbook on the Physics and Chemistry of Rare Earths, Elsevier, Amsterdam, 1987, p. 51.
[59] G. Armagan, A.M. Buoncristiani, B. Di Bartolo, Opt. Mater. (1992) 11.
[60] D.P. Neidirk, R.C. Powell, J. Lumin. 20 (1979) 261.
[61] Shiqi Liu, Yujun Liang, Miaohui Tong, Dongyan Yu, Yingli Zhu, Xingya Wu, Chunjie Yan, Mater. Sci. Semicond. Process. 38 (2015) 266–270.
[62] S.M. Berman, M. Navvab, M.J. Martin, J. Sheedy, W. Tithof, Light. Res. Technol. 38 (2006) 41.
[63] I.T. Kim, A.S. Choi, J.W. Jeong, Build. Environ. 57 (2012) 302.
[64] N. Ohta, A.R. Robertson, Colorimetry – Fundamental and Applications, John Wiley & Sons, Ltd., England, 2005.
[65] E. Fred Schubert, Light-Emitting Diodes, 2nd edn., Cambridge University Press, New York, 2006, p. 292.